Available online at www.sciencedirect.com
ScienceDirect
Journal of Catalysis 245 (2007) 84–90
JOURNAL OF CATALYSIS
www.elsevier.com/locate/jcat

Platinization of sunlight active Ti–W mixed oxide photocatalysts

M. Fernández-García [a,*], A. Fuerte [b], M.D. Hernández-Alonso [a], J. Soria [a], A. Martínez-Arias [a]

[a] *Instituto de Catálisis y Petroleoquímica (CSIC), C/Marie Curie 2, 28049-Madrid, Spain*
[b] *Departamento de Energía, CIEMAT, Av. Complutense, 28040-Madrid, Spain*

Received 28 July 2006; revised 25 September 2006; accepted 30 September 2006

Available online 27 October 2006

Abstract

The photocatalytic effects of the platinization on sunlight-active nanosize Ti–W mixed oxide materials with anatase structure were investigated. Platinization was shown to promote the photocatalytic mineralization of toluene, leading to an enhanced reaction rate of ca. 2.3 with respect to the parent Ti–W mixed oxide. This reaction rate increase is significantly higher than that obtained using ultraviolet excitation for titania-based oxides in the degradation of toluene and seems intimately related to the presence of Pt–O bonds located at the platinum–anatase interface. The chemical/physical bases of such behavior are discussed on the light of a structural/electronic characterization of the solids with the help of X-ray diffraction and Raman/UV–visible spectroscopy, along with additional in situ experiments run under sunlight excitation using infrared and electron paramagnetic resonance spectroscopy.

Keywords: Photocatalysis; Binary Ti–W mixed oxides; TiO_2; Anatase; Platinization; Visible and sunlight light absorption and excitation; Pollutant and toluene mineralization and degradation

1. Introduction

Photocatalytic destruction of organic pollutants in the presence of TiO_2 appears to be a viable decontamination process with widespread application, regardless of the state (gas or liquid) or chemical nature of the process target [1,2]. However, its technological applications seem limited by several factors, among which the most restrictive is the need to use an ultraviolet (UV) excitation source. The efficient use of solar light (i.e., the visible region of the spectrum) may then appear to be an appealing challenge for developing the future generation of photocatalytic materials. Among other possibilities, doping of TiO_2 materials with several cations, including V, Fe, W, and Mo, has been shown to be an effective way to enhance photoactivity under visible light excitation [3–10].

The photodeposition of platinum in its metallic state on titania surfaces is a well-known method of enhancing activity under ultraviolet light [11], but has yielded rather poor results when visible light is used as the energy source for decontamination processes [12]. Kisch and coworkers were successful in using Pt (and other metals) chlorides as visible light sensitizers but at the expense of slow degradation of the sensitizer, which ultimately could end in photoinstability [13]. Very recent results have shown, on the other hand, that Pt–TiO_2 interfaces become photoactive in parallel to the formation of Pt–O bonds with anions from the titania and concomitant oxidation of the noble metal [14]. This would suggest that oxidized or partially oxidized Pt states at the Pt–TiO_2 interface promote photoactivity and that preparation methods that promote the formation of Pt–O(TiO_2) contacts may be successful in improving this property. Platinization of TiO_2-based materials influences photoactivity by several factors; Lee and Mills [11] discussed causes related to the nature of the reactant–TiO_2 interaction (e.g., the adsorption of the pollutant and the oxidation/reduction of the pollutant/oxygen), whereas novel studies have been able to show a strong influence of the charge carrier behavior and lifetime, which in turn displayed a dependence on the TiO_2 material physicochemical characteristics [15].

In this paper we seek to gain insight into Pt–titania interfaces working under sunlight excitation by comparing the photocatalytic effects produced by oxide-type Pt-containing species on

* Corresponding author. Fax: +34 91 585 4760.
E-mail address: m.fernandez@icp.csic.es (M. Fernández-García).

0021-9517/$ – see front matter
doi:10.1016/j.jcat.2006.09.023

TiO_2 and W-doped TiO_2 catalysts prepared using the same method. A W doping level that maximizes photoactivity under sunlight excitation was chosen for this study [9]. We focus on the influence of the noble metal role on the W–Ti system and show a strong synergistic effect between Pt and the modified TiO_2-based material, leading to significantly improved photoactivity. Toluene photomineralization was chosen to test activity, because this is considered an important constituent of anthropogenic emissions in urban atmospheres. In addition, its photo-oxidation is a very demanding reaction and thus provides a tough chemical test to assess the potential of the TiO_2-based systems in the photoelimination of organic pollutants [8,9]. To shed some light on the role of noble metal, a study of the pollutant/oxygen interaction with the samples was conducted under reaction conditions in an in situ IR cell. The EPR spin-trapping technique, using DMPO as the spin-trap reagent, was applied to detect free hydroxyl-related radical intermediates generated during the visible irradiation process and assist in analyzing the charge carrier behavior.

2. Experimental

2.1. Sample synthesis and characterization

TiO_2 and W–TiO_2 (hereinafter called T and W, respectively) were prepared by microemulsion, giving oxide solids with anatase structure after calcination at 723 K for 2 h. Sample W corresponds to a $Ti_{0.81}W_{0.19}O_x$ substitutionally disordered solid oxide solution with cationic Ti vacancies to achieve charge neutrality. Table 1 summarizes the main preparation and physicochemical characterization parameters, which have been described elsewhere [9,16]. Pt was deposited by the incipient wetness method on the calcined oxide materials using nitrate salt (Merck) to a final solid content of 0.3 wt% (metal basis). Table 1 also gives the main preparation and physicochemical properties of Pt-containing samples.

The BET surface areas and average pore sizes were measured by nitrogen physisorption using a Micromeritics ASAP 2010 instrument. Particle sizes were measured by XRD using Scherer's equation. XRD profiles were obtained with a Seifert diffractometer using Ni-filtered Cu$K\alpha$ radiation. UV–visible diffuse reflectance spectroscopy experiments were performed with a Shimadzu UV2100 apparatus, and Raman data were acquired using a Bruker RFS-100 FT-Raman spectrometer.

Table 1
Conditions used in the thermal treatment and main characterization results

Sample	S_{BET} (m^2/g)	Average pore size (nm)	Crystal size (nm)[a]	Direct/indirect band gap (eV)	Preparation conditions
T	106	5.7	8.5	3.1/3.5	723 K[b]
TPt-3	82	4.7	8	3.0/3.5	723 K[c]
W	122	6.2	5	2.7/3.1	723 K[b]
WPt-1	84	5.3	5	2.7/3.0	523 K[c]
WPt-2	81	5.3	4	2.7/3.1	623 K[c]
WPt-3	76	5.1	4	2.6/3.1	723 K[c]

[a] For anatase-type structure. Measured by XRD.
[b] For 2 h under air.
[c] For 3 h under air.

2.2. Photoactivity measurements

Activity and selectivity for the gas-phase photo-oxidation of toluene were tested in a continuous-flow annular photoreactor [17] containing ca. 30 mg of photocatalyst as a thin coating on a Pyrex tube. The corresponding amount of catalyst was suspended in 1 ml of water, painted on a Pyrex tube (cutoff ca. 290 nm), and dried at room temperature. The reacting mixture (100 ml/min) was prepared by injecting toluene (Panreac, spectroscopic grade) into a wet (ca. 75% relative humidity) 20 vol% O_2/N_2 flow before entering the photoreactor at room temperature, yielding an organic inlet concentration of ca. 800 ppmv. After the mixture was flowed for 1 h (control test) in the dark, the catalyst was irradiated using four fluorescent daylight lamps (6 W, Sylvania F6W/D), with a radiation spectrum simulating sunlight (UV content of 3%), positioned symmetrically outside the photoreactor. Reference experiments with UV lamps (Sylvania F6WBLT-65, 6 W, maximum at ca. 350 nm) were run using the same reaction setup and procedure. Reaction rates were evaluated (vide supra) under steady-state conditions, typically achieved after 3–4 h from the start of irradiation. No change in activity was detected for any sample over the subsequent 6 h. The concentration of reactants and products was analyzed using an on-line gas chromatograph (HP G1800C) equipped with a HP5 capillary column (0.25 mm i.d. × 30 m) and a flame ionization detector using a SIM mode.

2.3. Fourier transform infrared (FTIR) measurements

For the infrared (IR) experiments, a Nicolet 5ZDX-FTIR spectrometer equipped with a MCT detector (4 cm^{-1} resolution) was used. The samples were pressed into a thin wafer (15 mg/cm^2) and placed in an IR Pyrex cell equipped with NaCl windows and greaseless stopcocks. The cell could be evacuated by connecting it to a conventional vacuum line (residual pressure: 1×10^{-4} Torr). Measured amounts of reactants (i.e., toluene and oxygen) could be introduced to the reactor cell. For irradiating the wafer, the IR cell was introduced into an apparatus similar in terms of lamp type and geometrical setup to that used for performing the photoactivity tests.

The IR spectra of two different samples (W and WPt-3) were recorded after the following treatments performed at room temperature: (i) evacuation for 2 h; (ii) dosing of 5 Torr of toluene (distilled in vacuum before use) into the IR cell and subsequent introduction of 50 Torr of oxygen; (iii) irradiation for 1 h; and (iv) evacuation of the sample for 15 min. Spectra were obtained after each of these four steps.

2.4. EPR experiments

The EPR measurements were done with a Bruker ER200D spectrometer operating in the X-band and calibrated with a DPPH standard. For the DMPO spin-trapping EPR experiments, the samples were suspended in water (at a concentra-

tion of 1 g/l) and sonicated for 4 min. An aqueous solution (0.01 M) of DMPO spin trap (supplied by Sigma) was prepared and kept on ice during the whole set of experiments. Bidistilled water (Elix-10) was used for these preparations. Then 100 μl of the solid suspension and 100 μl of the DMPO solution were mixed into an EPR flat quartz cell under atmospheric air and irradiated at different times through a Pyrex glass filter (cutoff at ca. 290 nm), with sunlight-type lamps identical to those used for the photocatalytic activity tests. The mixture was then immediately transferred to the spectrometer cavity for EPR analysis. A small radical concentration decay (ca. 5% on average) was observed in the dark during the course of spectrum recording. The recordings were obtained at 298 K by accumulating seven scans (in continuous mode, ca. 5 min of total recording time) at ca. 9.75 GHz microwave frequency, 19.5 mW microwave power, 100 kHz modulation frequency, 1 G modulation amplitude, and 2×10^5 spectrometer gain. No significant signal saturation was observed in those conditions. Blank experiments were also performed over mixtures of 100 μl DMPO solution and 100 μl water to check the absence of radical formation in the absence of solid under the conditions used.

3. Results and discussion

3.1. Structural and textural properties

Platinum deposition on the T and W oxide supports produces a detectable decrease in surface area even after calcination at low temperature (573 K; Table 1). It thus appears that some occlusion of the pore volume available to the gas phase occurred during platinum incorporation onto the support surface and/or subsequent calcination at the lowest temperature used in this work. In accordance with this suggestion, the measured average pore diameter decreased moderately in the presence of Pt for all samples (Table 1). At higher temperatures (673–723 K), no further significant structural/textural effects on the Ti-containing oxide phase were shown by the XRD/BET data presented in Table 1. This behavior was similar in both sample series (T and W) and occurred without the appearance of other TiO_2 polymorphs besides anatase, as confirmed by XRD (Fig. 1) and Raman spectroscopy (Fig. 2). The latter set a detection limit of <0.5 wt% for the presence of "impurity phases" (e.g., rutile and brookite) in the solids [18]. In addition, no changes were apparent in the Raman spectra after reaction (Fig. 2), indicating the stability of the Ti-containing phase under reaction conditions, as was observed previously for the bare supports [9]. According to TGA data of the WPt series (not shown), the calcination treatment produced weight losses at ca. 400, 550, and 630 K, as was observed previously and discussed by others [19]. Accordingly, our calcination temperatures were chosen to decompose the Pt precursor while trying to keep the number of Pt–O(TiO_2) contacts to a maximum. Calcination at 523 K (WPt-1 sample) may be a limiting case, however, in which some Pt–(NO_x) bonds likely remained on the surface of the material.

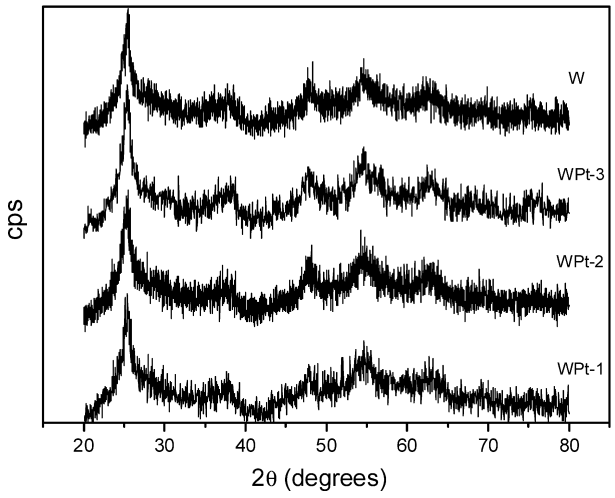

Fig. 1. XRD patterns for the W series of samples.

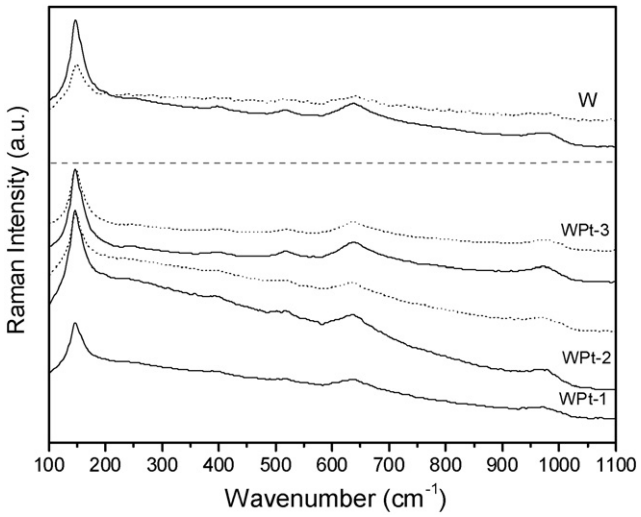

Fig. 2. Raman spectra for the W series of samples: (—) calcined samples; (···) post-reaction samples.

3.2. Toluene photocatalytic oxidation

The steady rate and selectivity to benzaldehyde values obtained with the T and W supports and Pt-containing samples as photocatalysts in the toluene gas-phase photocatalytic oxidation (PCO) are presented in Fig. 3a. Only CO_2 and benzaldehyde were detected during reaction as gaseous products. For comparison purposes, the values of both catalytic parameters obtained with the commercial P25 (anatase + rutile) are also included in this figure. Analysis of Fig. 3 reveals an enhanced toluene PCO steady rate and improved selectivity to CO_2 on doping the titania structure with tungsten, along with generally improved performance of the microemulsion-prepared oxides with respect to the P25 reference. This improvement, fully discussed previously [9], was attributed mainly to an enhanced visible light absorption by the W-containing photocatalyst. The presence of platinum influenced photoactivity in all cases. Concerning the T support, the TPt-3 sample displayed a significant increase in the selectivity to benzaldehyde, whereas the growth in PCO rate

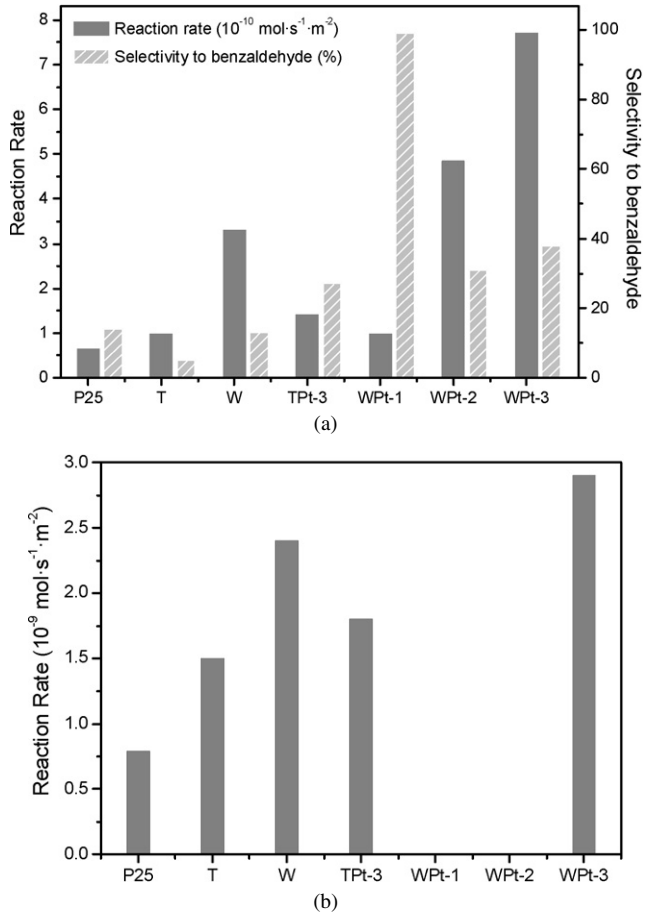

Fig. 3. (a) Reaction rates and selectivity to benzaldehyde of T and W series of samples in the gas-phase mineralization of toluene using sunlight type excitation; (b) reaction rate but using UV type excitation.

was small. Selectivity changes can be due to an increase in the number of sites where benzaldehyde is formed and/or to hampering of the benzaldehyde photo-oxidation process when platinum is incorporated onto the anatase surface. The rate increase (hereafter expressed as the I-factor, measured in this case as the TPt-3/T reaction rate ratio) was ca. 1.2, rather similar to the corresponding factor obtained under UV light (Fig. 3b) but somewhat inferior to the 1.3 value reported previously for platinization of P25 using UV excitation and obtained in the potential presence of metallic platinum [20].

For the W series, a strong dependence of the reaction rate was observed with the calcination temperature. Whereas a marked decrease of the reaction rate was observed for WPt-1 calcined at 523 K, a significant enhancement was measured for WPt-2 and WPt-3 calcined at 623/723 K, corresponding to I-factor (e.g., WPt-x/W reaction rate ratio) values of 1.5/2.3. Concomitant changes were detected in the selectivity of the reaction to benzaldehyde, which reached values close to 100% for WPt-3 and close to 35% for WPt-2 and WPt-3, slightly higher than that for TPt-3. These results suggest that in the W series, at calcination temperatures below 623 K, the presence of residual Pt–(NO_x) bonds from the precursor negatively influenced the reaction rate, deactivating the sites at which toluene mineralization occurred. On calcination at $T \geqslant 623$ K, we measured I-factors well above those typical for toluene mineralization in gas and liquid phases using UV excitation, around 1.2 (Fig. 3b), and in the 1.2–1.4 range in previous studies [11,20,21]. This increased toluene PCO with decreasing selectivity to benzaldehyde (with respect to WPt-1) indicates that the removal of the residual Pt–(NO_x) bonds and the concomitant formation of Pt–O(TiO_2) bonds originated at sites active for toluene mineralization and/or less affected by deactivation processes. These results show that for both series, T and W, platinum favored benzaldehyde formation and/or hampered its photo-oxidation, but the increased toluene mineralization to a level not reported previously is exclusively related to the combined presence of W and Pt.

The importance of the UV component of our sunlight-type source was calibrated with a parallel study of toluene mineralization using UV light (350 nm) as the excitation source. Although a moderate increase in the reaction rate was detected in the presence of tungsten for the T and W supports [9], the presence platinum in both series of samples yielded only a minor improvement (e.g., I-factors of 1.1–1.3), giving support to the idea that reaction changes under sunlight excitation are driven mainly by the visible part of the spectrum.

3.3. UV and FTIR spectroscopic studies

The creation of Pt–O(TiO_2) bonds on addition of platinum to the anatase materials produces no discernible effect on the UV–visible spectra reported for the T and W supports [22]. Table 1 contains band gap estimations considering either an indirect or a direct semiconductor, which display constant values within error (ca. 0.1 eV) of 3.5/3.1 eV for the T series of samples and 3.1/2.7 eV for the W series of samples. In addition, because platinum is in an oxidized state, the absence of metal surface plasmon bands that may allow visible light absorption was expected and was confirmed by UV–visible spectroscopy (not shown). The constancy of the band gap and the absence of Pt-metallic absorption features imply no gain of absorption power in the visible region from using our platinized samples with respect to the corresponding support counterparts.

To investigate Pt-related changes in reaction rate and selectivity, we first performed an IR study of the Pt chemical-type effects on the W series. Toward this end, Fig. 4 compares results for toluene adsorption and/or photoreaction with oxygen in the W support and the Pt-containing sample giving the highest I-factor (WPt-3). The spectrum of the fresh WPt-3 sample shows weak, ill-defined bands at ca. 1600 and 1450 cm^{-1} due to the presence of water and organic residues on the solid surface after calcination. The bands at around 1450 cm^{-1} are similar to those detected for the W support (result not shown; see [9]). Along with this spectrum, Fig. 4 also displays difference spectra to aid in interpreting changes occurring during every treatment step, as detailed in the Experimental section. On toluene adsorption, narrow bands were formed at ca. 1626, 1602, 1568, 1493, 1458, and 1378 cm^{-1}. The bands at 1602, 1568, and 1493 cm^{-1} can be assigned to the in-plane skeletal vibrations, whereas the bands at 1458/1378 cm^{-1} are associated with the asymmetric/symmetric CH_3 bending vibrations of

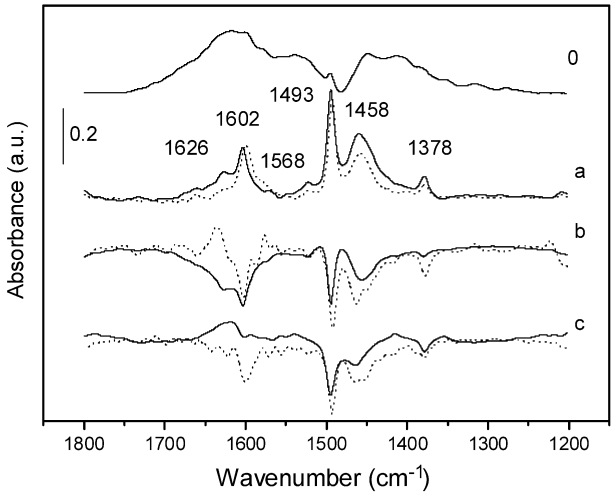

Fig. 4. IR difference spectra of WPt-3 (—) and W (- - -) samples following treatments: (0) fresh sample after 2 h of evacuation; (a) dosing 5 Torr of toluene and subsequent introduction of 50 Torr of oxygen; (b) sunlight irradiation for 1 h; and (c) evacuation for 15 min.

adsorbed toluene [23]. The in-plane skeletal vibrations are the IR modes most often considered in studying toluene adsorption. The downward shift of these bands, observed at 1615–1610 and 1502–1500 cm^{-1} for toluene in gas phase and at 1608–1605 and 1500–1494 cm^{-1} for liquid toluene, indicates a weakening of the ring C–C bonds due to the ring interactions. More marked downward shifts observed in adsorbed states indicate a stronger toluene ring interaction with an adsorbent surface. The red shift of the organic in-plane skeletal vibrations at 1602/1568/1493 cm^{-1} with respect to gas-phase wavenumbers leads us to conclude that the organic molecule is adsorbed by formation of a π-complex with surface cations, with their ring carbon atoms interacting with surface bridging oxygen [23]. However, the smaller shift of the band at 1602 cm^{-1} (with respect to the W support) may indicate that the aromatic ring of some other adsorbed toluene molecules is little affected by interactions with the support sites, likely because these toluene molecules are adsorbed through their methyl group. Concerning this last band, a word of caution may be warranted, because the presence of a significant amount of water (see below) may produce a small, but additional shift of band position with no correlation with the adsorptive properties of the solid surface. In any case, the detected differences between the spectra of the W and WPt-3 samples are related mainly to small variations in the red shift displayed by the in-plane skeletal vibrations. In addition, for WPt-3, a higher intensity of the band at 1625 cm^{-1}, corresponding to the bending mode of adsorbed water, was observed, probably caused by displacement of some adsorbed/created water molecules from toluene adsorption sites. This effect indicates that water (and/or related chemical groups) and toluene are competing for adsorption on the same sites, and that toluene adsorption seems energetically favored in the presence of platinum.

The subsequent irradiation of the W and WPt-3 samples caused a decrease in the toluene bands, but new bands, at ca. 1640, 1580, and 1225 cm^{-1}, corresponding to adsorbed benzaldehyde [24,25] were observed only in the absence of platinum (Fig. 4b). Considering the significant amount of benzaldehyde produced during toluene PCO on WPt-3 and its presence in the gas phase during IR experiments, this result indicates that benzaldehyde is weakly adsorbed on this sample, hindering further oxidation steps. Fig. 4b also shows the decrease in the band at 1626 cm^{-1}, indicating that the toluene PCO has allowed the water return to its previous adsorption site and/or to be simultaneously desorbed. In apparent accordance with the stronger toluene–surface interaction, a larger fraction of adsorbed toluene remained at the WPt-3 surface after irradiation in equilibrium with gas-phase toluene. Finally, after evacuation of the WPt-3 sample, we found positive peaks at 1625, 1420, and (very weak) 1320 cm^{-1}, attributable to bicarbonate ad-species [26,27], indicating that, as mentioned above, the region around 1625 cm^{-1} (and also around 1450 cm^{-1}) in fact contains contributions form several adsorbed species. This latter species was not observed previously in the T and W supports [9].

We can thus conclude that the presence of platinum strongly affects the chemistry of the organic molecule adsorption as well as its oxidation on irradiation while using a sunlight excitation source. A stronger adsorption of toluene is shown in parallel to a weaker adsorption of benzaldehyde and the presence of new products (e.g., not detected in the T and W samples), like bicarbonates. This suggests that Pt may contribute to decreasing stability of the aromatic ring by increasing its activation with a stronger interaction with the surface, followed by a rapid opening and formation of carbonates, while at the same time decreasing the relative stability of benzaldehyde and, probably, benzoate intermediates, which are believed to strongly poison TiO_2 surfaces [23,28–31]. Both factors may contribute to the enhanced reaction rate for toluene elimination under the specific conditions used in our reactor; the second factor is in agreement with a moderate increase in selectivity to aromatic oxygenates.

3.4. EPR study

Platinization has been also shown to influence the charge carrier balance and lifetime [15,32]. Here DMPO spin-trapping EPR experiments were carried out to detect free-radical intermediates generated during the irradiation process. Sunlight-type irradiation of DMPO-containing sample suspensions gave rise exclusively to a 1:2:2:1 quartet signal in the EPR spectra for all samples (Fig. 5a). Its EPR parameters ($g = 2.0056$, $a_N = 14.9$ G, and $a_H = 14.9$ G) are characteristic of DMPO–OH adducts formed on trapping of OH radicals by the DMPO molecules [22,33–35]. Evolution of the DMPO–OH signal with irradiation time is shown in Fig. 5b; the profiles generally show a maximum intensity that can be related to the limited stability of the radical adduct in an aqueous environment [34–36] or to the effect of multiple additions of hydroxyl radicals to the DMPO molecules, yielding diamagnetic molecules [35]. First, note that the generally lower overall intensity of DMPO–OH adducts is observed for the W-containing support with respect to the T reference, suggesting that the presence of W

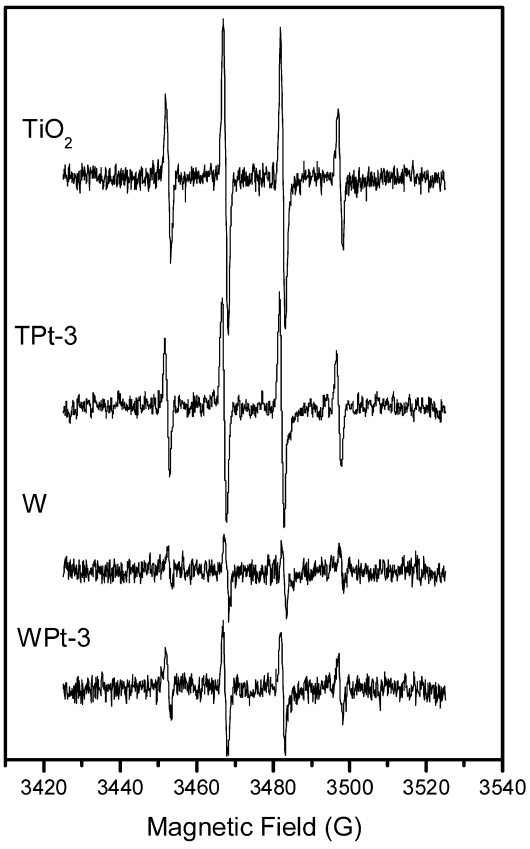

Fig. 5. (a) EPR spectra of the DMPO–sample aqueous suspension after 20 min sunlight irradiation; (b) evolution of the signal intensity with time.

hinders formation of OH radicals on photoexcitation to some degree.

In any case, the most interesting observation is the fact that platinization influences the production of OH radicals in different ways for T- and W-supported samples; whereas in the first case it seems to decrease photogeneration of hydroxyls significantly, the opposite effect is noted in the W-supported sample. As stated earlier, aromatic photo-oxidation initially yields benzaldehyde and other reactive intermediates in subsequent/parallel steps [30,31,37]. It appears that different hydroxyl groups can be involved in these steps; formation of benzaldehyde has been related to isolated species, whereas interaction with H-bonded hydroxyls may lead to further oxidation and ring opening of the organic molecule [30]. With the DMPO probe molecule, we are able to show the effect of platinization on the whole population of hydroxyl radicals (e.g., hydroxyl species capturing holes), thus limiting the information that we can extract from such an experiment to interpret mechanistic details. However, the experiment does provide evidence that platinization strongly alters charge carrier balance and lifetime and makes it in a significant different way in the T- and W-supported samples. This is in agreement with the work of Emilio et al. [15], who used time-resolved microwave conductivity to show that platinization always influences charge carrier lifetime in TiO_2 samples and suggested that both positive and negative effects occur in the charge carrier recombination lifetime and thus that detrimental and beneficial photocatalytic effects are induced by different compensation effects, which are related to the physicochemical properties of the solid in a way that was unclear up to now. Therefore, the observed DMPO-EPR experimental differences indicate that differences in the pollutant–surface chemistry between the W support and the WPt-3 sample could result from differences in charge carrier lifetime and behavior.

4. Conclusion

In this work we have investigated the promotional effect produced by adding platinum to a nanosized Ti–W mixed oxide with anatase structure in the photomineralization of toluene using sunlight excitation. The strong reaction rate increase detected (as measured by the I-factor) is significantly superior to that found under UV excitation for P25 and other TiO_2-based systems, and is associated with the influence of the Pt–anatase (oxide–oxide) interface in the solid properties. The combined presence of W/Pt into/onto the titania anatase structure yields an increase of the reaction rate of about one order of magnitude with respect to the parent nanoparticulate TiO_2 system, providing a clear, effective way to improve photocatalytic performance under sunlight excitation.

The presence of the noble metal in an oxidized state apparently does not change the structural (e.g., anatase size and surface) and electronic (e.g., band gap and optical characteristics) properties of the anatase-type nanosized Ti–W mixed oxide, although, according to DMPO-EPR experiments, it certainly influences charge carrier separation and behavior. The new charge carrier balance achieved in the presence of platinum produces clear chemical effects, as detected by in situ infrared experiments. The present study showed easier ring opening of the benzene fragment under reaction conditions, which, together with a limitation of the partial oxidation product(s) surface coverage(s), would be directly responsible for the enhanced reaction rate.

Acknowledgments

Financial support was provided by the CYCIT (project CTQ2004-03409/BQU). The authors thank Dr. E. Sastre, Dr. C. Belver, and R. Bellod for performing some of the experiments.

References

[1] J.-M. Herrmann, Top. Catal. 34 (2004) 49.
[2] M.R. Hoffmann, S.T. Martin, W. Choi, D.W. Bahnemann, Chem. Rev. 69 (1995) 95.
[3] W. Choi, A. Termin, M.R. Hoffman, Angew. Chem. Int. Ed. 33 (1994) 1091.
[4] D. Chatterjee, S. Dasguple, J. Photochem. Photobiol. C Rev. 6 (2005) 185.
[5] V. Brezová, A. Blazková, L. Karpinsky, J. Groskova, B. Havlínová, V. Jorík, M. Ceppan, J. Photochem. Photobiol. A Chem. 109 (1997) 177.
[6] M. Anpo, Stud. Surf. Sci. Catal. 130 (2000) 157.
[7] H. Yamasita, Y. Ichihashi, M. Takeuchi, S. Kishiguchi, M. Anpo, J. Synchrotron Rad. 6 (1999) 451.
[8] A. Fuerte, M.D. Hernández-Alonso, A.J. Maira, A. Martínez-Arias, M. Fernández-García, J.C. Conesa, J. Soria, Chem. Commun. (2001) 2178.
[9] A. Fuerte, M.D. Hernández-Alonso, A.J. Maira, A. Martínez-Arias, M. Fernández-García, J.C. Conesa, J. Soria, J. Catal. 212 (2002) 1.
[10] Q.X. Dai, H.Y. Xiao, W.S. Li, Y.Q. Na, Appl. Catal. A 290 (2005) 25.
[11] S.-K. Lee, A. Mills, Platinum Met. Rev. 47 (2003) 61.
[12] H. Arakawa, K. Sayama, Res. Chem. Intermed. 26 (2000) 145.
[13] W. Macyk, H. Kisch, Chem. Eur. J. 7 (2001) 1862, and references therein.
[14] D. Lahiri, V. Subramanian, B.C. Bunker, P.V. Kamat, J. Chem. Phys. 124 (2006) 204720.
[15] C.A. Emilio, M.I. Litter, M. Kunst, M. Bouchard, C. Colbeau-Juntin, Langmuir 22 (2006) 3606.
[16] M. Fernández-García, A.J. Martínez-Arias, A. Fuerte, J.C. Conesa, J. Phys. Chem. B 109 (2005) 6075.
[17] A.J. Maira, K.L. Yeung, J. Soria, J.M. Coronado, C. Belver, C.Y. Lee, V. Augugliaro, Appl. Catal. B 29 (2001) 327.
[18] E. Murad, H.M. Koster, Clay Miner. 34 (1999) 479.
[19] M. Schneider, M. Wildberger, M. Maciejewski, D.G. Duff, T. Mallat, A. Baiker, J. Catal. 148 (1994) 625.
[20] M.C. Blount, J.L. Falconer, J. Catal. 200 (2000) 21.
[21] K.A. Magrini, A. Watt, B. Rinehart, Solar Eng. (1995) 415.
[22] A. Fuerte, M.D. Hernández-Alonso, A. Iglesias-Juez, A. Martínez-Arias, J.C. Conesa, J. Soria, M. Fernández-García, Phys. Chem. Chem. Phys. 5 (2003) 2913.
[23] M. Nagao, Y. Suda, Langmuir 5 (1989) 42.
[24] A. Méndez-Roman, R. Cardona-Martínez, Catal. Today 40 (1998) 353.
[25] G. Martra, Appl. Catal. A 200 (2000) 275.
[26] P. Primet, J. Phys. Chem. 86 (1982) 4708.
[27] G. Busca, H. Saussey, O. Saur, J.C. Lavalley, V. Lorenzelli, Appl. Catal. 14 (1985) 245.
[28] Y. Luo, D. Ollis, J. Catal. 163 (1996) 1.
[29] L. Cao, Z. Gao, S.L. Suib, T.N. Obee, S.O. Hay, J. Catal. 196 (2000) 253.
[30] A.J. Maira, J.M. Coronado, V. Augugliaro, K.L. Yeung, J.C. Conesa, J. Soria, J. Catal. 202 (2001) 413.
[31] Y. Irokawa, T. Morikawa, K. Aoki, S. Koska, T. Ohwaka, T. Taga, Phys. Chem. Chem. Phys. 8 (2006) 1116.
[32] P. Pitchar, J. Disdier, J.M. Hermann, Nov. J. Chim. 6 (1982) 559.
[33] D.L. Haire, Y. Kotake, E.G. Janzen, Can. J. Chem. 66 (1988) 1901.
[34] M.A. Grela, M.E.J. Coronel, A.J. Colussi, J. Phys. Chem. 100 (1996) 16940.
[35] D. Dvoranová, V. Brezová, M. Mazur, M.A. Malati, Appl. Catal. B 37 (2002) 91.
[36] E.G. Janzen, N. Sankuratry, Y. Kotake, J. Magn. Reson. 111 (1996) 254.
[37] M.C. Blount, J.F. Falconer, Appl. Catal. B 39 (2002) 39.